EFFECT OF CONTINUOUS DAMAGE DEACTIVATION ON YIELD AND FAILURE SURFACES

Marcin CEGIELSKI*, Artur GANCZARSKI*

* Institute of Applied Mechanics, Dept. of Mechanical Engineering, Cracow University of Technology, Al. Jana Pawła II 37, 31-864 Kraków

Artur.Ganczarski@pk.edu.pl

Abstract: This article deals with the modeling of the continuous damage deactivation affected yield surfaces of copper and failure surfaces of mortar, from the viewpoint of continuum damage mechanics. The concept of damage deactivation is adapted to Tresca-Guest and Huber-Mises surfaces and two models are presented: the classical discontinuous one, in which microcracks close instantaneously, and the new continuous one, in which they close gradually. The results for both models are compared and verified in order to achieve the best fitting the experimental data. Detailed quantitative and qualitative analysis of obtained solutions confirms the necessity and correctness of an application of the continuous damage deactivation concept.

1. INTRODUCTION

Degradation of a material leads to a change of mechanical properties of it such that: decrease of the material stiffness described by modified constants of elasticity, decrease of the material strength, which can be described by appropriate strength criterion of damaged material and growth of the material anisotropy resulting from directional nature of damage effects.
Therefore the constitutive equations of damage material should include aforementioned effects and they also should be reducible to the equations valid for the initial state when growth of material degradation has not been initiated. Considering the strength condition of damaged material our investigation are limited to the simplified case when undamaged material is isotropic. Consequently, the strength condition is understood here as a state when either the yield condition is fulfilled or ultimate stress is reached. The strength condition may be presented as the following scalar function

$$f(\boldsymbol{\sigma}, D) = 0, \tag{1}$$

where $\boldsymbol{\sigma}$ stands for the stress tensor and D describes isotropic damage parameter, which vanishes in case of the undamaged material. Graphical interpretation of Eq. (1), presented schematically in Fig. 1, performs certain limit surface defined in stress space, which shrinks and deforms due to damage. The decrease of material strength with damage can be explained in such a way that achievement of limit surface in the undamaged material requires stress σ_{ij} (vector $0A$), whereas in case of damaged material the appropriate stress σ^*_{ij} is essentially smaller (vector $0A_1$).

Limit surfaces play fundamental role in the generalized theories of plasticity–damage (see Lemaitre and Chaboche 1985, Lemaitre 1992) and creep-damage phenomena (see Litewka 1991), where they serve as the dissipation potentials. Hence, two postulates are crucial for the question, whether a given limit surface may be applied as the dissipation potential used in theories based on generalized associated flow rule: f is a scalar continuous or partly conti-nuous (having at most finite set of corner points) and convex function of its arguments.

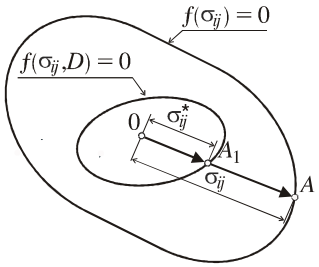

Fig. 1. Change of the limit surface due to damage

2. REVIEW OF EXPERIMENTAL DATA

2.1. Isochronous creep rupture curves for copper

Isochronous creep rupture curves or, in other words, curves of identical time to rupture, are very convenient graphical interpretation of the fracture criterion accompanying creep. Usually, these curves are drawn in the principal stress co-ordinate system and each point of the subsequent curve represents the stress level leading to rupture, after time characteristic for this curve is reached.

Relatively the highest number experiments in the field of rupture accompanying creep under biaxial stress state was done for copper at 523 K (see Finnie and Abo el Ata 1971, Johson et al. 1956, Murakami and Sanomura 1985, Murakami et al. 1986), which enabled Litewka (1991) to compare their results for several magnitudes of rupture time (Fig. 2).

Detailed analysis of subsequent isochronous creep rupture curves did not confirm assumption of invariant shape, initially noticed by Broberg (1975), and allowed Litewka (1991) to formulate hypothesis that, depending on the level of stress, they may approach either Huber-Mises ellipses (higher magnitude of stress) or Tresca-Guest hexagon (lower magnitude of stress).

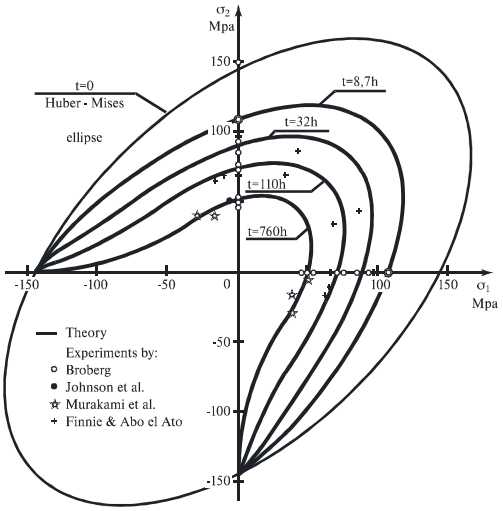

Fig. 2. Isochronous creep rupture curves for copper at temparture 523 K (after Litewka 1991)

2.2. Mortar damage loading surfaces

The mechanical behavior of masonry was subject of several experimental studies by Page (1981, 1983), Dhanasekar et al. (1985), Rots (1997) and van der Pluijm (1999). Experimental failure envelope shape, obtained in uniaxial tension, uniaxial compression, biaxial compress-ion under medium confinement, triaxial compression under medium confinement and hydrostatic compression, is presented in Fig. 3. The failure envelope is much more sensitive in tension than in compression (*k* stands for ratio of compressive/tensile strength).

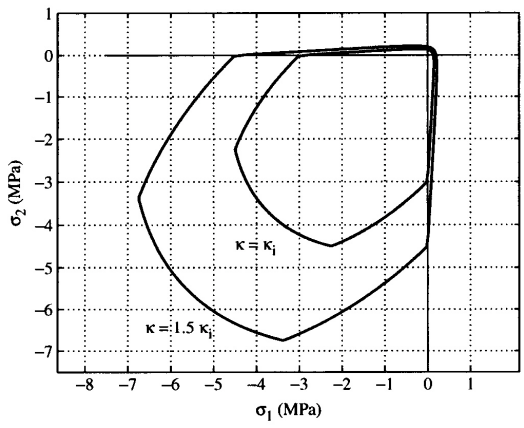

Fig. 3. Mortar damage loading surfaces (after Page 1991, 1993, Dhanasekar et al. 1985, Rots 1997 and van der Pluijm 1999)

3. LIMIT SURFACES AFFECTED BY DAMAGE

3.1. Discontinuous damage deactivation

In what follows, modeling of damage influence on Tresca-Guest or Huber-Mises limit surfaces is directly associated with the kinetic theory of damage evolution proposed by Lemaitre and Chaboche (1985) and Lemaitre (1992). Key point of this theory is the limit surface treated as the yield potential referring to theory of associated plasticity and built on the basis of effective stress concept. In general case, damage is anisotropic phenomenon usually described by the second order tensor. However, in order to make derivations possible, the simplest isotropic damage is assumed and the effective stress equals to

$$\tilde{\boldsymbol{\sigma}} = \boldsymbol{\sigma} / (1 - Dh), \tag{2}$$

where D stands for damage and h denotes crack closure opening parameter. Such simplified scalar description of damage does not allow for distinction of microcrack orientation but, simultaneously, it is sufficient to trace influence of damage closure on change of the macroscopic properties of material.

Direct substitution of Eq. (2) into Eq. (1) shows that the form of yield potential essentially differs in case of tension, when damage is active, than in case of compression, when damage remains inactive. This phenomenon is called damage deactivation and its description requires to take into account the parameter h

$$h = \begin{cases} 1 & \text{tension} \\ 0 & \text{compression} \end{cases} \tag{3}$$

As consequence, in case of the plane stress state and under assumption that damage is active if at least one of stress components is positive ($\sigma_1>0$ and/or $\sigma_2>0$) or, in other words, h=1 if Tr$<\boldsymbol{\sigma}>=<\sigma_1>+<\sigma_2>$ is positive. The Macauley brackets <.> are defined as $<x>=0.5(x+|x|)$. In the Tresca-Guest case yield potential takes following form

$$\begin{aligned} &\Sigma_1 = 1 - D \quad \Sigma_2 = 1 - D && \text{in } 1^{\text{st}} \text{ quarter} \\ &\Sigma_1 = -1 \quad \Sigma_2 = -1 && \text{in } 3^{\text{rd}} \text{ quarter} \\ &\Sigma_1 - \Sigma_2 = \pm(1 - D) && \text{in } 2^{\text{nd}} \text{ and } 4^{\text{th}} \text{ quarters} \end{aligned}, \tag{4}$$

whereas in the case of Huber-Mises

$$\Sigma_1^2 - \Sigma_1\Sigma_2 + \Sigma_2^2 = \begin{cases} (1-D)^2 & \text{in } 1^{\text{st}}, 2^{\text{nd}}, 4^{\text{th}} \text{ quarters} \\ 1 & \text{in } 3^{\text{rd}} \text{ quarter} \end{cases}, \tag{5}$$

where $\Sigma_i = \sigma_i / \sigma_y$ is dimensionless stress (σ_y denotes yield stress) which turns out to be non-smooth and non-convex function (see Figs 4, 5). Namely, for any nonzero damage state (here D=0.6) there exist two linear segments ($0A_1$ and $0B_1$ for Tresca-Guest hexagon, or A_1A_2 and B_1B_2 for Huber-Mises elipse), corresponding to instantaneous damage deactivation that link together appropriate segments of second and third or third and fourth quarters, respectively.

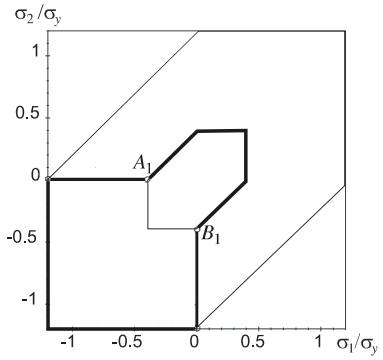

Fig. 4. Tresca-Guest yield surface in case of discontinuous damage deactivation effect (D=0.6)

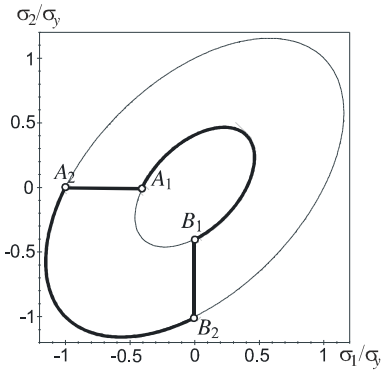

Fig. 5. Huber-Mises yield surface in case of discontinuous damage deactivation effect (D=0.6)

3.2. Continuous damage deactivation

The aforementioned defect of the yield potential Eqs (4-5) may successfully be removed by introducing continuous damage deactivation, when microcracks do not close instantaneously but gradually like which is schematically shown in Fig. 6 (see Hansen and Schreyer 1995, Foryś and Ganczarski 2002, Ganczarski and Barwacz 2007, Ganczarski and Cegielski 2007)

$$h(\boldsymbol{\sigma}) = h_{\mathrm{c}} + (1-h_{\mathrm{c}})\chi(\boldsymbol{\sigma})/\chi(\boldsymbol{\sigma}_{\mathrm{b}}), \tag{5}$$

where h_{c} stands for the critical magnitude of damage deactivation parameter (assumed for simplicity equal to 0.0), $\boldsymbol{\sigma}_{\mathrm{b}}$ denotes stress referring to the full microcrack opening and $\chi(\boldsymbol{\sigma})$ is the Hayhurst function

$$\chi(\boldsymbol{\sigma}) = \alpha \mathrm{Tr}(\boldsymbol{\sigma}) + (1-\alpha)J_2(\boldsymbol{\sigma}), \tag{6}$$

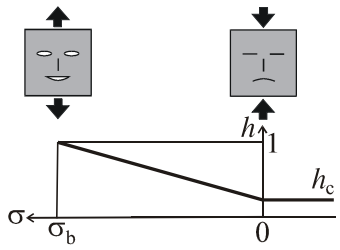

Fig. 6. Graphical interpretation of continuous damage deactivation

Restricting considerations to the simplified case when $\chi(\boldsymbol{\sigma})$ depends only on positive value of the first invariant of stress tensor α=1 and $\mathrm{Tr}(\boldsymbol{\sigma})=\mathrm{Tr}\langle\boldsymbol{\sigma}\rangle$ and assuming, additionally, that microcracks are fully opened under maximum tension

$$\sigma_{\mathrm{b}} = \begin{cases} (1-D)\sigma_{\mathrm{y}} & \text{points } A_1 \text{ and } B_1 \text{ at Tresca hexagon} \\ \dfrac{2(1-D)\sigma_{\mathrm{y}}}{\sqrt{3}} & \text{points } A_1 \text{ and } B_1 \text{ at Mises ellips} \end{cases}, \tag{7}$$

and closed completely under compression (h_{c}=0 at points 0 or A_2 and B_2, respectively), the yield surfaces are given by formulas: the Tresca-Guest case

$$\begin{aligned} &\Sigma_1 = 1-D \quad \Sigma_2 = 1-D && \text{in } 1^{\text{st}} \text{ quarter} \\ &\Sigma_1 = -1 \quad \Sigma_2 = -1 && \text{in } 3^{\text{rd}} \text{ quarter} \\ &\Sigma_1 - (1+\tfrac{D}{1-D})\Sigma_2 = -1 && \text{in } 2^{\text{nd}} \text{ quarter} \\ &(1+\tfrac{D}{1-D})\Sigma_1 - \Sigma_2 = 1 && \text{in } 4^{\text{th}} \text{ quarter} \end{aligned}, \tag{8}$$

and the Huber-Mises case

$$\Sigma_1^2 - \Sigma_1\Sigma_2 + \Sigma_2^2 = \begin{cases} (1-D)^2 & \text{between points } A_1 \text{ and } B_1 \\ (1-\dfrac{D}{1-D}\dfrac{\sqrt{3}}{2}\Sigma_2)^2 & \text{between points } A_1 \text{ and } A_2 \\ (1-\dfrac{D}{1-D}\dfrac{\sqrt{3}}{2}\Sigma_1)^2 & \text{between points } B_1 \text{ and } B_2 \\ 1 & \text{in } 3^{\text{rd}} \text{ quarter} \end{cases}, \tag{9}$$

schematically shown in Figs 7 and 8.

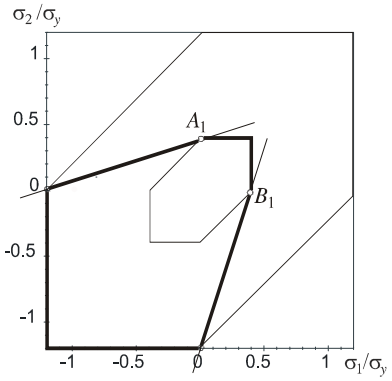

Fig. 7. Tresca-Guest yield surface in case of continuous damage deactivation effect (D=0.6)

New yield surfaces are composed of either two segments of the Tresca hexagon joined by two straight lines or the Mises ellipses linked together by two hyperbolas, becoming parabolas in particular case of $D=2\sqrt{3}/(3+2\sqrt{3})\approx 0.5358$. Subsequent stages of damage affected yield surfaces shown in Figs 9 and 10 exhibit qualitatively and quantitatively good agreement with experimental investigations demonstrated in Figs 2 and 3. In comparison to curves presented in Figs 4 and 5 the convexity and smoothness (except finite set of points) are recovered, hence they both may serve as damage affected yield potentials: the Tresca-Guest hexagon for modeling of metallic materials subjected to lower magnitudes of stress

and the Huber-Mises ellipses for modeling of both metallic materials subjected to higher magnitudes of stress and concrete or rock like materials.

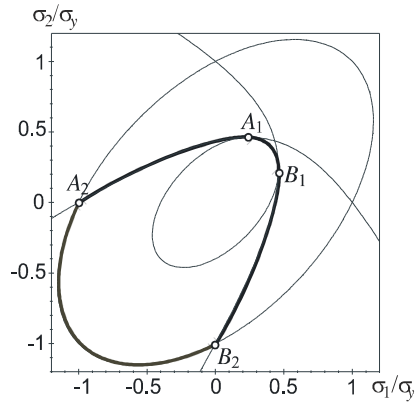

Fig. 8. Huber-Mises yield surface in case of continuous damage deactivation effect (D=0.6)

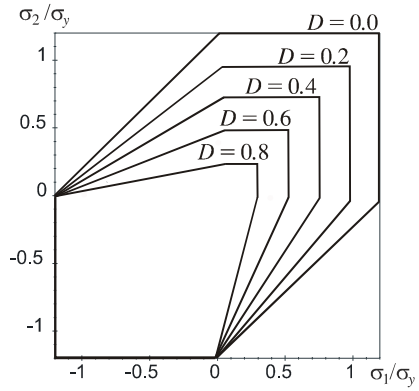

Fig. 9. Subsequent stages of damage affected Tresca-Guest yield surface by use of continuous damage deactivation

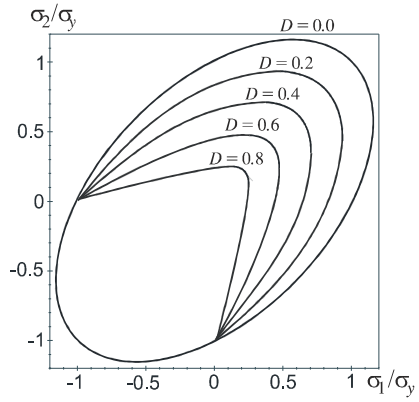

Fig. 10. Subsequent stages of damage affected Huber-Mises yield surface by use of continuous damage deactivation

4. CONCUSIONS

1. Modeling of limit surfaces by use of the classical discontinuous damage deactivation leads to insufficient mapping of complex experimental data revealing physically unjustified discontinuities.

2. Application of the continuous damage deactivation concept gives both quantitatively and qualitatively good agreement with the experimental data, and confirms necessity and correctness of this approach in modeling of damage affected limit surfaces of copper and mortar.

REFERENCES

1. **Broberg H.** (1975) Creep damage and rupture, a phenomenological study, PhD Thesis, Chalmers Tekniska Högskola, Göteborg.
2. **Dhanasekar M., Page A.W., Kleeman P.W.** (1985), The failure of brick masonry under biaxial stresses, in *Proc. Instn. Civ. Engrs., Part 2*, 295-313.
3. **Finnie I., Abo el Ata M.M.** (1971), Creep and creep-rupture of copper tubes under multiaxial stress, in *Advances in Creep Design*, eds. Smith A.J., Nicolson A.M., Willey, New York, 329-352.
4. **Foryś P., Ganczarski A.** (2002), Modelling of microcrack closure effect, Proc. *Int. Symp. Anisotropic Behaviour of Damaged Materials* (on CD ROM).
5. **Ganczarski A., Barwacz L.** (2007), Low cycle fatigue based on unilateral damage evolution, *Int. J. Damage Mechanics*, Vol. 16, No 2, 159-177.
6. **Ganczarski A., Cegielski M.** (2007), Efekt ciągłej deaktywacji uszkodzenia, *Acta Mechanica et Automatica*, Vol. 1, No 1, 35-38.
7. **Hansen N.R., Schreyer H.L.** (1995), Damage deactivation, *Trans. ASME*, 62, 450-458.
8. **Johson A.E., Henderson J., Mathur V.D.** (1956), Combined stress fracture of commercial copper at 250^{o}C, *The Engineer*, 24, 261-265.
9. **Lemaitre J., Chaboche J.-P.** (1985), *Mécanique des matériaux solides*, Bordas, Paris.
10. **Lemaitre J.** (1992), *A course on damage mechanics*, Springer-Verlag, Berlin Heidelberg.
11. **Litewka A.** (1991), Damage and fracture of metals in creep conditions, Thesis of Poznań University of Technology, No 250 (in Polish).
12. **Murakami S., Sanomura Y.** (1985), Creep and creep damage of copper under multiaxial states of stress, in *Plasticity today*, eds. Sawczuk A, Bianchi G., Elsevier, London, 535-551.
13. **Murakami S.**, **Sanomura Y., Saitoh K.** (1986), Formulation of cross-hardening in creep and its effect on the creep damage process of copper, *J. Eng. Mat. Techn.*, 108, 167-173.
14. **Page A.W.** (1981), The biaxial compressive strength of brick masonry, *Proc. Instn. Civ. Engrs., Part 2*, 71, 893-906.
15. **Page A.W.** (1983), The strength of brick masonry under biaxial tension-compression, *Int. J. Masonry Constr.*, 3, 26-31.
16. **Rots J.G.** (1997), *Structural masonry-an experimental-numerical basis for practical design rules*, Balkema, Rotterdam.
17. **van der Pluijm R.** (1999), *Discontinuous modelling of strain localisation and failure*, PhD Thesis, Delft Univ. Techn.

ACKNOWLEDGEMENTS

Authors gratefully acknowledge the support rendered by the State Committee for Scientific Research, KBN, Poland, Project PB-807/T07/2003/25.